J Mater Sci: Mater Med (2014) 25:283–295
DOI 10.1007/s10856-013-5071-6

Bioactivation of calcium deficient hydroxyapatite with foamed gelatin gel. A new injectable self-setting bone analogue

M. Dessì · M. A. Alvarez-Perez · R. De Santis · M. P. Ginebra · J. A. Planell · L. Ambrosio

Received: 14 September 2013 / Accepted: 9 October 2013 / Published online: 18 October 2013

Abstract An alternative approach to bone repair for less invasive surgical techniques, involves the development of biomaterials directly injectable into the injury sites and able to replicate a spatially organized platform with features of bone tissue. Here, the preparation and characterization of an innovative injectable bone analogue made of calcium deficient hydroxyapatite and foamed gelatin is presented. The biopolymer features and the cement self-setting reaction were investigated by rheological analysis. The porous architecture, the evolution of surface morphology and the grains dimension were analyzed with electron microscopy (SEM/ESEM/TEM). The physico-chemical properties were characterized by X-ray diffraction and FTIR analysis. Moreover, an injection test was carried out to prove the positive effect of gelatin on the flow ensuing that cement is fully injectable. The cement mechanical properties are adequate to function as temporary substrate for bone tissue regeneration. Furthermore, MG63 cells and bone marrow-derived human mesenchymal stem cells (hMSCs) were able to migrate and proliferate inside the pores, and hMSCs differentiated to the osteoblastic phenotype. The results are paving the way for an injectable bone substitute with properties that mimic natural bone tissue allowing the successful use as bone filler for craniofacial and orthopedic reconstructions in regenerative medicine.

M. Dessì (✉) · M. A. Alvarez-Perez · R. De Santis · L. Ambrosio
Institute of Composite and Biomedical Materials, National Research Council of Italy, P.le Tecchio 80, 80125 Naples, Italy
e-mail: M.Dessi2@brighton.ac.uk

Present Address:
M. Dessì
School of Pharmacy & Biomolecular Sciences, University of Brighton, Lewes Road, Brighton BN2 4GJ, UK

Present Address:
M. A. Alvarez-Perez
Faculty of Dentistry, National Autonomous University of Mexico (UNAM), Circuito Exterior s/n, Coyoacan, 04510 Mexico, DF, Mexico

M. P. Ginebra · J. A. Planell
Department of Materials Science and Metallurgy, Technical University of Catalonia, Av.Diagonal 647, 08028 Barcelona, Spain

J. A. Planell
Institute for Bioengineering of Catalonia, Baldiri Reixach, 10-12, 08028 Barcelona, Spain

1 Introduction

A crucial step within the field of bone tissue-engineering is the use of materials that conceivably recreate a spatially organized bone extra cellular matrix (ECM). These burgeoning mainstays stimulate in vivo tissue ingrowth acting as temporary matrix for cell guidance [1]. Because of pivotal role of the ECM in morphogenesis tissue, the basic strategy of the recent tissue-engineering attempts is closely mimicking the physiological environment [2]. An appropriate material for bone repair should face transversal properties including geometrical, mechanical and topographical features, and promote the biunivocal cell-ECM cross-talks, fostering the right ECM type production [3, 4]. The bioactivation process elegantly conveys the materials response to external cues towards the integration with surrounding environment and the new tissue formation. Bioceramics like Calcium Phosphates (CaP) attract great interest in this field due to their similarity to the minerals in natural bone and their excellent biocompatibility and bioactivity [2–9]. In some specific formulations, their

outstanding osteoconduction capability matches the ability to be molded and injected into osseous sites, forming an in situ self-setting scaffold [5–8], which can be resorbed and replaced by new bone. The biomimetic approach, with the pursuit of developing a superior matrix that synergizes the beneficial properties of multiple materials, solves the brittleness of ceramic by adding biopolymers that resemble the organic part of bone. Gelatin is a high molecular weight polypeptide derived from collagen, highly biocompatible, completely resorbable in vivo and skillful at enhancing cell adhesion [10]. It possesses an amphiphilic character that allows it to be easily foamed, and coupling with CaPs improves the workability of cement and its mechanical properties [11–13]. The incorporation of a bioactive phase promotes cell-surface recognition, cell physiology and cellular affinity of the scaffold, inducing a biological fixation between scaffold and biological milieu. However, such composites often lack the balance between morphological and mechanical properties [4]. To overcome the aforementioned limitations, here we have used a novel approach based on the use of gelatin as porogenic agent in α-tricalcium phosphate (α-TCP) cement, without the use of organic solvents that alter cellular activity. In this way, is possible to increase the porosity of material and pores interconnectivity useful for cell colonization, molecular transport and tissue growth, while preserving mechanical properties. This work is aimed to obtain a challenging injectable in situ self-setting material that intimate fits complex cavity, with different features able to sustain cell activity. The ensuing cement sets at body temperature through a hydrolysis reaction, which final product is calcium deficient hydroxyapatite (CDHA) that resembles the human apatite crystals [14]. A careful investigation of the rheological properties of gelatin gel and the kinetic of setting were carried out. The Environmental Scanning Electron Microscopy was used to investigate the morphological changes upon time. Injection tests at body temperature were performed to demonstrate the injectability enhancement in presence of the foamed biopolymer. Moreover, a morphological characterization (SEM/TEM) has been carried out to investigate the macro/micro-porosity and crystals dimension. The physico-chemical analysis was performed by X-ray and FTIR, and thermal stability and mechanical properties of the hardened material were assessed. Preliminary biological analysis has been evaluated with MG63 and hMSCs cells, to assess the suitability of the material for bone regeneration applications.

2 Materials and methods

The calcium phosphate powder of the cement (HCem) consisted of 98 % by weight of α-TCP and 2 wt% of precipitated hydroxyapatite (PHA), added as a seed to enhance the nucleation of the CDHA resulting as setting reaction product. Bovine gelatin type B (isoelectric point = 5, Bloom strength = 250) sterilized with γ-ray was kindly provided by Ghent University. Gelatin powder was dissolved (15 % w/v) at 40 °C under gently stirring in 2.5 % (w/v) aqueous solution of Na_2HPO_4, used as accelerant solution for the setting reaction of the cement. The foaming process was carried out at 40 °C by foaming the gelatin solution 1 min per ml at 11,000 rpm with a home-made mixer on 1.5 V. Foamed and not foamed gelatin solutions were used as liquid phase of cement at a Liquid/Powder ratio (L/P) of 0.75.

2.1 Rheological analysis

Rheological tests were performed in a rotational rheometer (Gemini, Bohlin Instruments) equipped with parallel plate and coaxial cylinders geometry, at the controlled temperature of 37 ± 0.01 °C in humid environment to prevent evaporation during the measurements. The rheological properties were evaluated in terms of shear storage modulus or elastic modulus (G'), and shear loss modulus or viscous modulus (G''). G' gives information about the elasticity or the energy stored in the material during deformation, whereas G'' describes the viscous character or the energy irreversibly dissipated [15–18]. The temperature dependence of G' and G'' was determined by temperature scan at constant frequency of 0.5 Hz and constant shear strain 0.05 in order to evaluate the transition temperature. The viscosity η as function of shear rate was evaluated both for foamed and not foamed hydrogels, through steady state shear measurements at 37 °C with shear rate spanning from 0.1 to 110 s^{-1}. The paste injected was subjected to a dynamic single frequency sweep in order to evaluate the evolution setting kinetic 2 min after the injection.

2.2 Injection test and mechanical characterization

Cement pastes were extruded at 37 °C using a bioinjector device, equipped with a 5 ml syringe with a 12G needle, at a crosshead speed of 40 mm min^{-1}. The injectability (I %) is defined as the percentage of extruded mass with respect to the original mass of paste in the syringe. After hardening (12 days in accelerant solution) static compressive properties tests were performed following ASTM D 695 by using a universal testing machine INSTRON4204, equipped with 100 N load at cross-head speed of 1 mm min^{-1} at 37 °C. The Young Modulus (E), the maximum compressive strength (σ_{max}) and the maximum deformation (ε_{max}) of each tested sample were obtained.

2.3 Thermal analysis and contact angle measurements

Thermal gravimetric analysis (TGA) was performed on TA Instruments Q500, USA. under nitrogen atmosphere at a purge rate of 50 ml min^{-1}, from room temperature up 600 °C and heating rate of 10 °C min^{-1}. The hydrophilicity of the samples was assessed by contact angle measurements on the material surfaces by the sessile drop technique, at 25 °C using a Contact angle analyzer Electrictime CO.ING., Natick, Mass, USA. Static water contact angles were measured by deposing on the foamed composite surface, a droplet (2 µl) of bidistilled water [18–20].

2.4 Phase and microstructures characterization

A qualitative morphological examination was performed in order to investigate the evolution of the surface morphology of the sample in solution over the setting, as well as the internal structure of the specimens. This enables the indirectly examination of the interrelationship between mechanical properties and microstructures. Specimens were cut along the transversal section and Environmental Scanning Electron Microscopy (ESEM) was performed after 24, 48, 96 h and 14 days. For a complete observation of the pores, samples were dried and then sputtered with gold for SEM studies. Both observations were performed in Quanta 200 FEI scanning electron microscope. The ultrastructural evaluation analysis was performed with Philips EM 208 s Transmission Electron Microscope (TEM). Fourier transform infrared (FTIR) spectroscopy (Nicolet 5700) was used to determine the functional groups of the composite and their single constituents and the possible bonds between the ceramic and polymer phases in the composite material. 2 mg of powder were compacted with 200 mg of KBr in a hydraulic press. Spectra were recorded in the 400–4,000 cm^{-1} region [21]. Phase analysis of the synthesized composites was conducted by X-ray diffraction (XRD) to determine the phase composition and crystallinity with an X-ray diffractometer (Philips PW1710). The powder specimens were scanned from $2\theta = 5$ to $2\theta = 60$ using Cu Ka radiation [22].

2.5 Biological studies

Cell viability and proliferation were carried out on osteoblastic lineage MG63, while mesenchymal stem cells hMSCs were used to investigate the osteogenic differentiation and the osteoinductive and osteoconductive features of the material. Each experiment was performed three times in triplicate.

Cylindrical sterile scaffolds were pre-wetting in medium (2 h) and 5×10^4 cells, resuspended in 50 µl of medium, were statically seeded on the scaffolds. After seeding the scaffolds were placed in 24-well culture plates and incubated for 2 h in a humidified atmosphere.

2.5.1 Alamar blue assay

Proliferation of MG63 was quantitatively determined by Alamar Blue assay (AbD Serotec Ltd., UK). Cell–scaffold constructs were removed from the culture plates on days 1, 3 and 7, rinsed with PBS and placed in 24-well culture plates. Accordingly with literature procedures [21–24], for each construct 1 ml of Dulbecco's modified Eagle's medium (DMEM) without Phenol red (HyClone, UK) containing 10vol. % Alamar blue was added, followed by incubation in a 5 % CO_2 atmosphere for 4 h at 37 °C. An aliquot of 200 µl of the solution was subsequently removed and the optical density was measured with a Sunrise spectrophotometer (Tecan, Männedorf, Switzerland) at wavelengths of 540 and 600 nm.

2.5.2 DNA quantification and alkaline phosphatase (ALP) assay

The hMSCs–scaffold constructs were removed from culture plates on days 7, 14 and 21 and washed with PBS. DNA amounts in the 3D porous scaffolds were determined by using DNA assay, PicoGreen dsDNA quantification kit (Molecular Probes). Firstly, 100 µl of 200× diluted Picogreen dsDNA quantification reagent was added to 100 ml of cell lysate in a 96-well plate. After 10 min incubation, the fluorescence of Picogreen was determined at a wavelength of 520 nm after excitation at 585 nm as described by manufacturer [21–25]. For ALP assay cells were lysed in Cell Lysis Buffer (BD Pharmingen™) and ALP activity was measured using a SensoLyte™pNPP alkaline phosphatase assay kit (AnaSpec,DBA,Milano) according to the manufacturer's instructions. The ALP activity was read off a standard curve obtained with ALP concentrations of 0–200 ng ml^{-1}.

2.5.3 In vitro osteogenic differentiation and detection of osteoblasts markers

hMSC cells were cultured in osteogenic medium consisting of complete α-MEM medium supplemented with 50 µg ml^{-1} of ascorbic acid, 10 mM glycerol-2-phosphate and 10^{-7}M of dexamethasone. For in vitro osteogenic assay, after seeding hMSC were placed in 24 cell culture plates and allowed to attach overnight in standard α-MEM medium. Then, cells were grown in presence of osteogenic medium for 14 days, while control culture scaffolds were grown in standard α-MEM medium without osteogenic supplements. After 14 days, hMSC cultures onto composite cement grown in osteogenic and control medium were

characterized by reverse transcription-polymerase chain reaction (RT-PCR) for gene expression of bone-related markers. Total RNA was isolated from cell scaffolds using TRI-reagent (SIGMA). The RNA was precipitated with isopropyl alcohol and the final pellet resuspended in DEPC-water and DNAse I digested (Invitrogen Carlsbad, CA) to remove contaminating of genomic DNA. The absorbency at 260/280 nm was measured to determine the RNA concentration. One μg of total RNA was used to perform one-step RT-PCR reaction (Invitrogen Carlsbad, CA) according to the manufacturer's protocol. Bands were visualized using ultraviolet illumination and captured with BioRad Imaging System (BIORAD).

2.5.4 Immunostaining

hMSC cultures onto composite scaffolds grown in control and osteogenic medium for 14 days were fixed with 4 % paraformaldehyde and permeabilized with PBS containing 0.1 % Triton X-100. Cells were incubated at 4 °C overnight in a 1:300 dilution of the rabbit (IgG) polyclonal antibody against human osteopontin and collagen type I in PBS containing 2 mg ml^{-1} of bovine serum albumin (BSA). The samples were washed with ice-cold PBS and incubated for 1 h at 4 °C with goat-anti-rabbit immunoglobulin secondary antibodies conjugated with FITC (3 mg ml^{-1}, Sigma Chemical, St. Louis, MO), diluted 1:100 in PBS. Samples were rinsed with PBS plus 0.01 % Triton X-100 three times and immunostaining were visualized by confocal laser scanning microscopy (LSM510; CarlZeiss).

2.5.5 Cell-material interaction

Experiments were performed to explore cellular morphology, spreading and colonization 14 days after seeding. Cells were fixed in 4 % paraformaldehyde for 1 h at room temperature and rinsed with PBS. For SEM analysis, samples were dehydrated in a graded series of ethanol, then dried, sputter coated with gold and observed with Quanta 200 FEI microscope. For confocal analysis, samples were incubated with PBS–BSA 0.5 % to block nonspecific binding. Actin microfilaments were stained with phalloidin tetramethylrhodamine B isothiocyanate (Sigma–Aldrich, Italy). Phalloidin was diluted in PBS–BSA 0.5 % and samples were incubated for 30 min at room temperature, then rinsed with PBS and observed by confocal laser scanning microscopy (LSM510; CarlZeiss).

3 Statistical analysis

Data are presented as mean ± standard deviation. Mean values were compared with one way ANOVA with respect to statistical significances ($P < 0.05$).

4 Results

4.1 Rheological analysis

In Fig. 1a G'and G" of gelatin solutions are charted as function of temperature. At low temperature samples show a gel-like behaviour with G'>G". On warming, the cross-over of the curves occurs and the moduli rapidly drop up

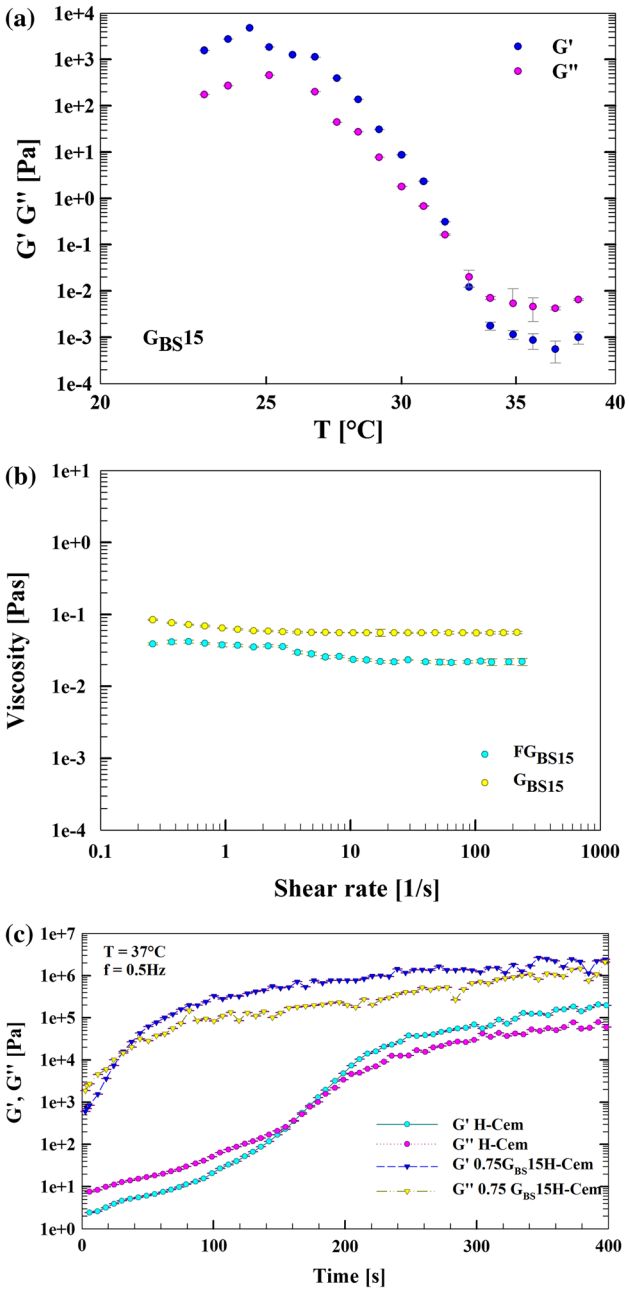

Fig. 1 Thermal scanning test of sterilized gelatin gel $G_{BS}15$ (*a*). Flow curves of foamed $FG_{BS}15$ and unfoamed $G_{BS}15$ sterilized gelatin gels (*b*), and time evolution of G' and G'' of composite foamed F0.75G_{BS}15HCem and cement without polymeric phase, HCem (*c*)

Table 1 Injection parameters of HCem, composite cement and foamed composite cement

Sample	Load (N)	Injection (%)
0.75 HCem	30 ± 0.3	59 ± 0.1
0.75 G_{BS}15 HCem	36.2 ± 0.06	85 ± 0.8
F0.75 G_{BS}15 HCem	34.4 ± 0.02	100

Table 2 Mechanical properties of HCem, foamed and unfoamed composite cements

Sample	σ_{max} (MPa)	E (GPa)	ε_{max} (%)
0.75 HCem	23 ± 3	0.8 ± 0.2	0.04 ± 0.01
0.75 G_{BS}15 HCem	2.9 ± 0.6	0.9 ± 0.3	7.5 ± 0.8
F0.75 G_{BS}15 HCem	3 ± 0.2	1.0 ± 0.1	9 ± 0.2

values of five orders of magnitude. The crossover temperature (T = 32 °C ± 0.05) indicates the transition from an elastic network to viscous solution (G"＞G'). This phenomenon has to be ascribed to the disruption of gelatin physical crosslinks or junction zones. At body temperature gelatin gels exhibit a behaviour intermediate between a strong gel and a viscous liquid, which positively affects both the workability and cohesion of composite cement. In order to obtain a highly porous composite, gelatin was foamed. Figure 1b shows the flow behavior of gelatin solutions foamed and not: within the shear rate range investigated, both samples show a newtonian behavior. Although the same gelatin concentration, the viscosity of foamed hydrogel was found to be lower than unfoamed hydrogel. Data show that bubbles disruption during the flow implies a decreasing of the friction among the slides of fluid, resulting in viscosity decrease. Rheological dynamic time sweep provided a monitoring of the build-up of cement network. By the analysis of the moduli charted as a function of time in Fig. 1c, the morphological evolution of the cement can be observed. Upon injection pastes possess fluid consistence with G"＞G', then the moduli rise towards a plateau value. The increase of G' in the sample without gelatin is lower than the foamed composite cement, which demonstrates that gelatin improves material cohesion. Moreover, the incorporation of polymeric phase improves the capacity of setting in a paste with elastic properties comparable to natural tissue [26, 27].

4.2 Injection test and mechanical characterization

The results of injectability test are shown in Table 1. In the cement paste without gelatin I % was found to be about 60 %. This limited injectability could be ascribed to phase separation or early hardening. The presence of polymeric phase implies a noteworthy increasing of paste injection: 85 % for composite with gelatin, 100 % for composite with foamed gelatin. Indeed, when gelatin is foamed, the injectability increases, due to the synergistic effect of gelatin presence and the porosity introduced by the foaming process. Table 2 lists the mechanical properties of the cement (100 wt% HCem) compared with foamed and not foamed composites. The presence of polymeric phase lowers the maximum compressive strength and increases the maximum deformation. In particular, the bubble's volume due to foaming technique strongly affects the increasing of cement ductility, as confirmed by the increasing of ε_{max} %. The brittle behaviour of ceramics is reduced thanks to the organic phase, which increases either workability or toughness of cement. In agreement with literature data [26, 27], the elastic modulus is similar to the value of natural bone tissue.

4.3 Thermal analysis and contact angle measurements

The changes in mass loss as function of temperature are reported in the termogravimetric trace in Fig. 2a. From the thermogram can be clearly noticed that the cement exhibits a degradation process based on different stages. The first weight loss of 3.45 %, observed in the temperature range of 75–100 °C, is due to water evaporation. The second weight loss between 100 and 150 °C should be ascribable to an unreverse reaction that leads to the loss of bound water molecules from structure. The major weight transition between 200 and 400 °C, with a mass loss of 4.45 %, can be directly attributable to the thermal degradation of biopolymer, based on the decomposition of gelatin triple helix structure. Furthermore, the residual calcium phosphate level at 400 °C, equal to 94 %, is consistent with the theoretical gelatin weight fraction used during preparation. Regarding contact angle measurements, intrinsically related to the topological cues explicated by the material, the resulting value of 25° is indicative of a highly hydrophilic character. Data obtained are lower than those reported in literature for hydroxyapatite, which are close to 50° [28, 29]. This confirms the hydrophilic behavior of foamed scaffold, simultaneously due to the active cue of gelatin and a more porous structure. The foamed polymeric phase has a significant impact not only on the injectability, also improves topographic features, such as wettability. The effect is essential in the first part of cell-material interaction, with significant influence on cellular recognition and scaffold adhesion.

4.4 Phase and microstructures characterization

The XRD pattern of composite powder shown in Fig. 2b underlines that after 12 days of setting the cement had

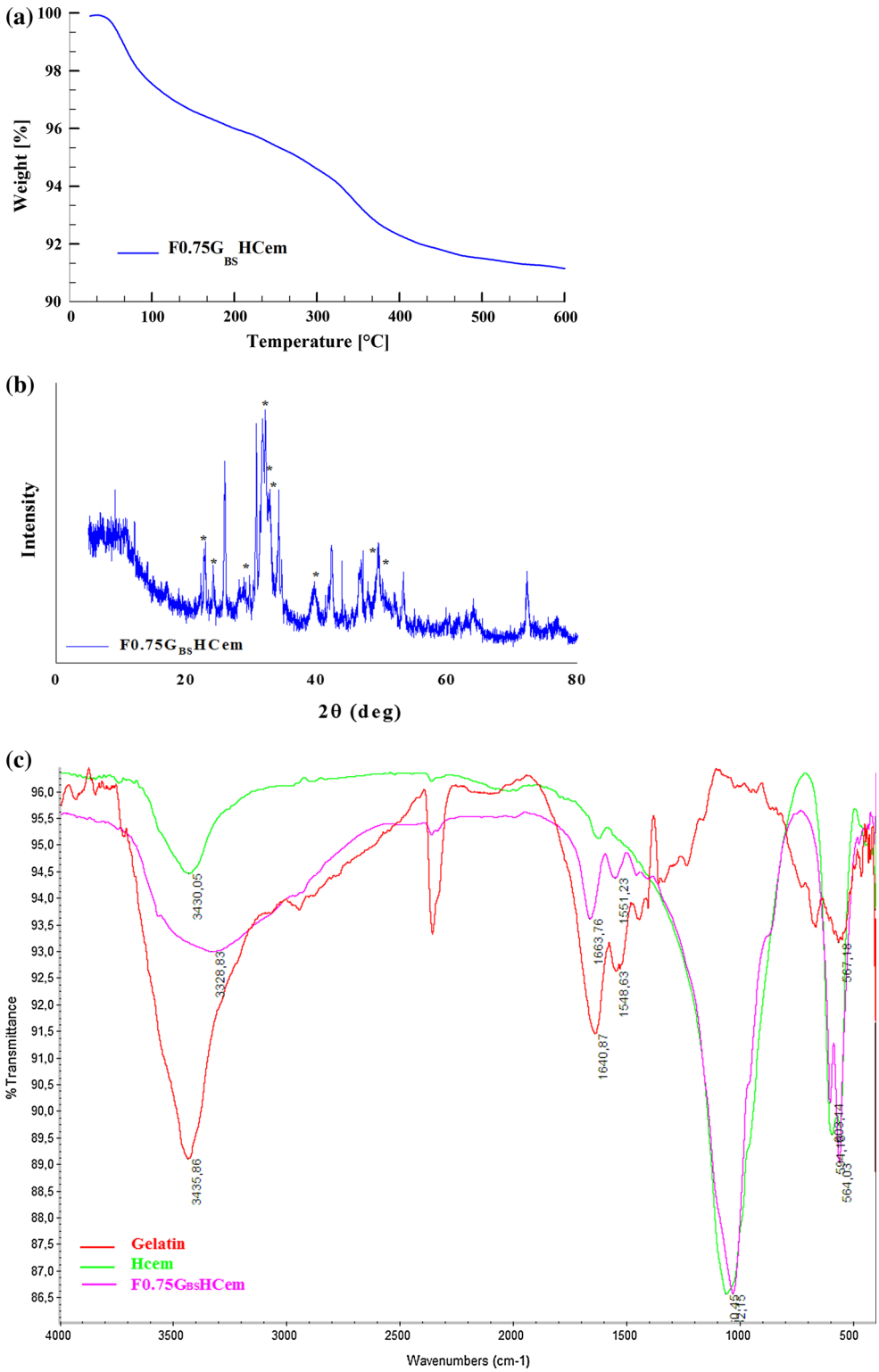

Fig. 2 Thermal analysis of foamed composite paste (*a*). X-ray spectrum of foamed composite cement (*CDHA) (*b*). FTIR spectra of gelatin, HCem powder and foamed composite cement (*c*)

completed the hydrolysis reaction, and the α-TCP has been conversed in CDHA, although slight residual amounts of α-TCP are still detected. The broad XRD peaks are indicative of a poor crystallinity degree. Many studies have reported that a poor crystallinity increases the bioactivity of hydroxyapatite, leading to a faster and stronger bond with the surrounding tissue [28]. The FTIR spectra of the gelatin, HCem, and composite cement are shown in Fig. 2c. For gelatin, the band at 1,640 cm^{-1} is representative of the amide I region of the protein and is chiefly linking to the

stretching vibrations of the carbonyl groups along the polypeptide backbone [12, 30–32]. The amide II region can be found at 1,520–1,550 cm^{-1}, while as reported in literature [12, 31–35] the amide III bands of the polypeptidic chain are depicted in the frequencies range at 1,100, 1,270–1,300, 1,229–1,235 and 1,243–1,253 cm^{-1}. The field at 3,435 cm^{-1} is dominated by N–H bond-stretching mode. With regard to ceramic phase, the spectrum shows well defined peaks at 950, 980 and 1,100 cm^{-1}, due to the ν_1 symmetric stretching bond and ν_3 vibrational modes of phosphates groups, while bands at 3,570, 630 and 480–600 cm^{-1} correspond to hydroxyl and phosphates groups [36, 37]. In the spectrum of foamed cement the evidence of CDHA is proven by HPO_4^{2-} bands at above 900 and 1,090 cm^{-1} [36, 38]. Moreover, the peak assigned to 470, 562 and 602 cm^{-1} result from doubly and triply degenerate O–P–O bending mode. The weak shoulder at 963 cm^{-1} is attributed to the non degenerate P–O symmetric stretching mode, while the broad band at 1,050 cm^{-1} indicates the triply degenerated antisymmetric P–O stretching mode [36–39]. The absorption band between 3,100 and 3,400 cm^{-1} is due to the O–H stretching. The intensity of the band around 3,400 and 1,600 cm^{-1} in composite is smaller compared to gelatin. From these results, since type B gelatin possess isoelectric point in the range of 5–6 and the biopolymer is negatively charged at physiological pH, the interaction between gelatin and ceramic phase could result from hydrogen bonding and/or by the formation of carboxyl–calcium–carboxyl linkages. The observation of time conversion of α-TCP into CDHA in situ is shown in ESEM micrographies in Fig. 3. After 24 h, polymeric phase is evident and round particles

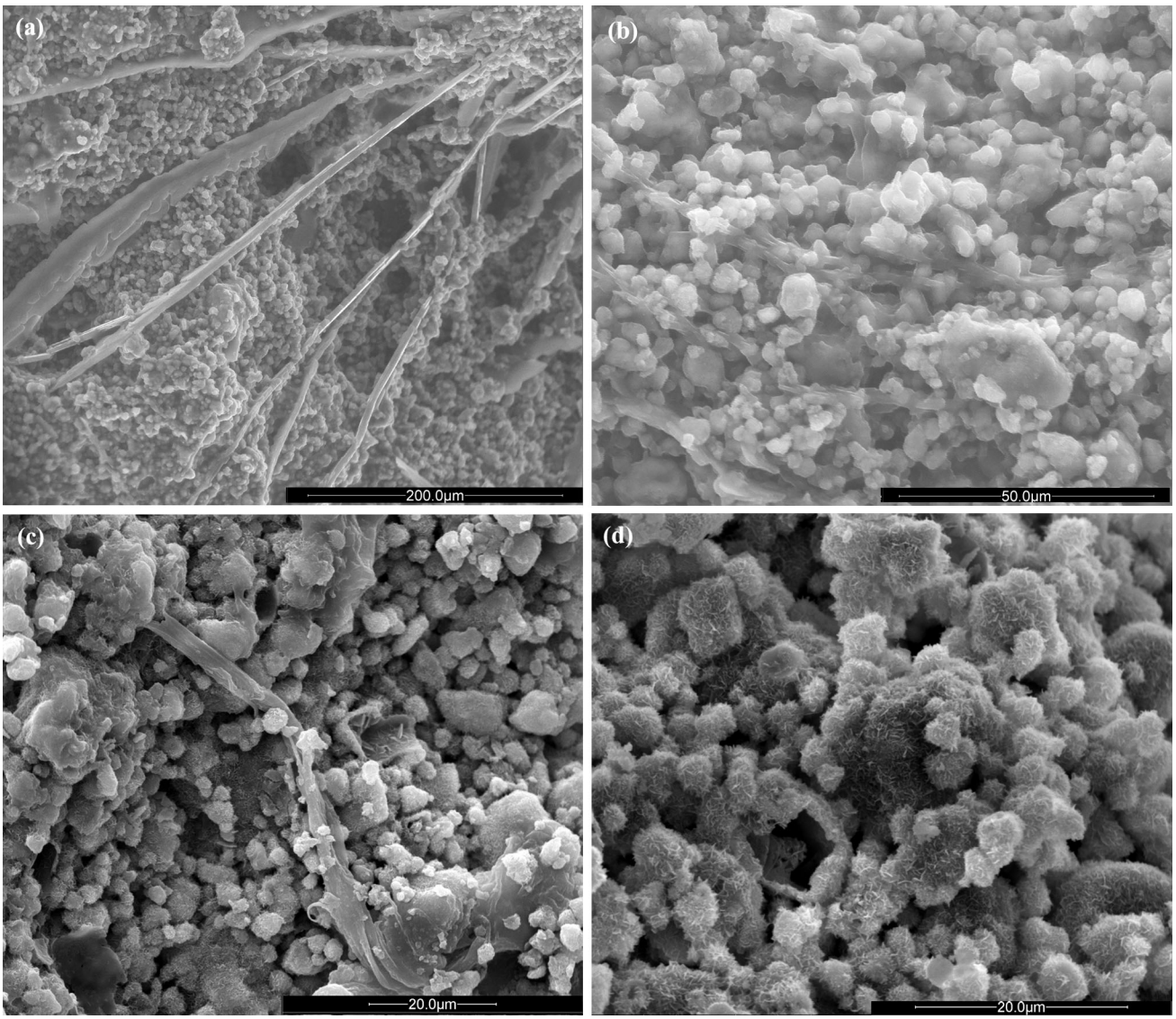

Fig. 3 ESEM micrographies representing the ingrowth of CDHA crystals carried out at 24 h (*a*), 48 h (*b*), 96 h (*c*) and 14 days (*d*)

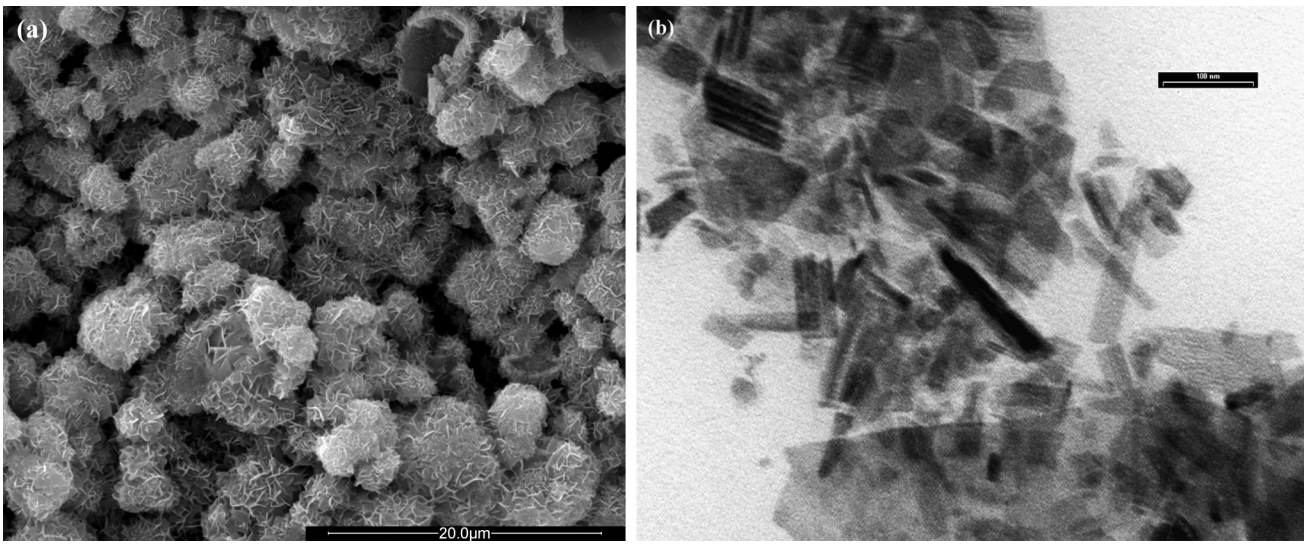

Fig. 4 SEM analysis of the inner surface of foamed composite cement (*a*). TEM micrograph of CDHA crystals (*b*)

of α-TCP are homogeneously distributed into the polymer network with a stochastic orientation; after 48 h small needle like crystals of CDHA appear, due to the dissolution of the small α-TCP particles, while the bigger ones are still surrounded by a layer of polymeric phase and calcium phosphate crystals. After 96 h of reaction, CDHA needle-like crystals are almost uniformly distributed into the network due to the hydrolysis in progress of α-TCP, although laminar compact crystals are present. After 14 days the phase conversion is completed and the surface is homogeneously covered by needle like crystals. SEM analysis shows the presence of a macro and microporosity characterized by average pore sizes of microns able to support cells deposition and to regulate the nutrient transport for cell viability. The micrography in Fig. 4a confirms a large distribution of CDHA crystals of needle shape homogeneusly distributed within the inner surface. TEM examination of the powders reveals the formation of crystallites of essentially acicular shape. Closer inspection puts the stress on the presence of needle-like like crystal well defined in geometry, thin, homogeneously and finely distributed. The micrography reported in Fig. 4b shows that the obtained powders are constituted by an average particle size in the range of 10–100 nm in length and 1–20 nm in thickness. These dimensions mimic the topological and morphological characteristics of natural HA and are optimal for the spreading and cellular migration [40].

4.5 Alamar blue assay

The Alamar Blue assay (Fig. 5) proves that after 7 days of static culture cells are vital and proliferate. Indeed, cells are attached onto scaffolds and their metabolic activity tends to increase over 7 days. From the trend reported in the

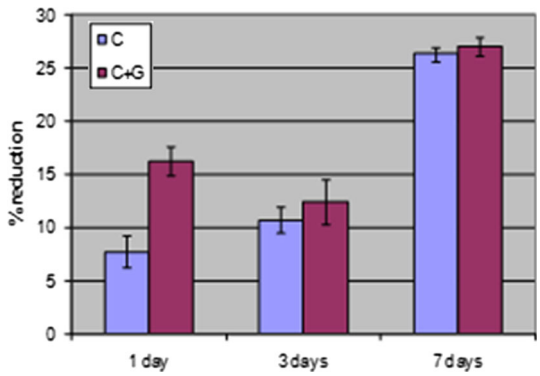

Fig. 5 Cellular viability and proliferation were determined by Alamar Blue assay performed on MG63 seeded on HCem (control, C) and gelatin foamed cement (C+G) cultured after 1, 3 and 7 days

histogram, it can be noticed that at day 1 the % of AB reduction on foamed composite cement is three times higher than the HCem used as control, then for both samples a significant increase in viability can be observed within 7 days. However the control and the composites exhibit similar values at 7 days. These data could be explained as the ability of gelatin to enhance cellular adhesion and proliferation without adversely affect cellular viability in the first stage of the process. It is clear that there is no cytotoxic effect of both scaffolds, and the proliferation guidance decreases at 7 days for a partial leaching of gelatin into the medium.

4.6 DNA quantification and alkaline phosphatase (ALP) assay

DNA quantification of hMSCs plotted in Fig. 6a shows that during the in vitro static culture the amount of DNA detected on the composite cement is significantly ($P < 0.05$) greater

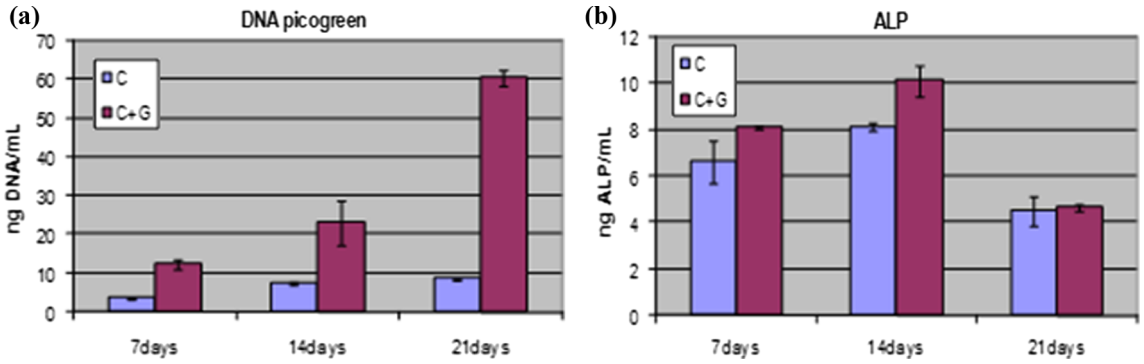

Fig. 6 Growth curves of hMSC cultured onto HCem (control, C) and foamed cement scaffolds (C+G) after 7, 14 and 21 days determined by DNA quantification assay. Cells of the foamed composite cement groups proliferated at each time point checked compared to control group that reached a plateau after 14 days of culture (*a*). ALP activity of hMSC measured on control HCem and foamed cement scaffolds after 7, 14 and 21 days of differentiation. ALP activity was significantly higher on foamed cement scaffold than on control surfaces (*b*)

than the control. It might be due to the presence of gelatin that exhibits excellent cell adhesion and proliferation properties and to the higher porous surface that offers sites for cells colonization. Cell differentiation assessed in terms of the ALP activity is plotted in Fig. 6b, and support DNA data. It can be observed that ALP activity for both samples increases up to days 14, where it reaches the maximum value, and then decreases. The gelatin foamed presence significantly enhances ($P < 0.05$) the hMSCs differentiation through 14 days, respect to HCem and cells express higher levels of ALP bone marker. After 21 days, when the gelatin is dissolved the values of ALP expression are comparable ($P > 0.1$). The depicted increasing in ALP activity suggests the ability of the composite scaffold to successfully support hMSC differentiation towards the osteoblast phenotype.

4.7 In vitro osteogenic differentiation and detection of osteoblasts markers

Figure 7a illustrates the RT-PCR of osteoblastic gene expression on hMSCs cultured after 14 days. In osteogenic medium hMSCs differentiated to osteoblasts within 14 days. Cells express high levels of genes of ospteopontin, alkaline phosphatase and type I collagen in presence of osteoinductive substrate. Furthermore, osteogenic medium induces cells changing phenotype, but RNA expression of collagen I and osteopontin are also expressed for cells growth in absence of osteoinductive factors. Since the expression of osteoblastic marker happens regardless the osteogenic nature of medium, by semi-quantitative RT-PCR assay the material can be defined osteoinductive.

4.8 Immunostaining

To test whether material surface characteristics alone are able to stimulate osteogenic differentiation, hMSC were

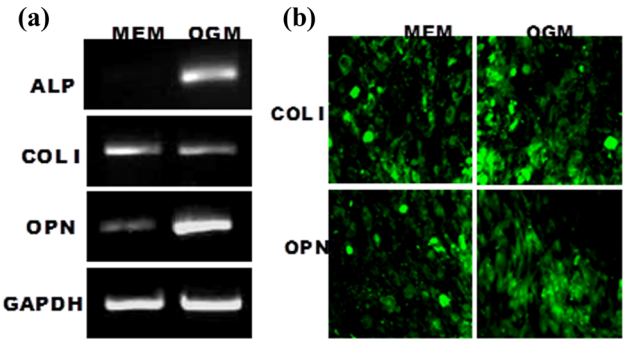

Fig. 7 Representative gel electrophoresis bands stained with ethidium bromide of the osteoblastic gene expression phenotype (alkaline phosphatase, osteopontin and collagen type I) detected by RT-PCR (*a*) and by CLSM immunostaining (*b*)

cultured on the material surface with and without osteogenic medium. Our results showed high level of osteopontin and type I collagen proteins expression detected by immunofluorescense as reported in Fig. 7b, in media with and without any osteogenic signal. Cells "feel" the features of materials and reply developing the osteoblastic phenotype, in this contest the scaffolds could be defined as osteoconductive.

4.9 Cell-material interaction

SEM images of the seeding surfaces and cross-sections of the cell–scaffold constructs are reported in Fig. 8. After 14 days of in vitro culture, hMSCs colonize the surface of the scaffold adhering into the macroporosity. Further, cells are well distributed around pores, spread with flattened and spindle shape and create several bridges between the opposite pore walls. Cells interacting each other by the presence of physical contact zone or junction zones, and are anchored to nanocrystals of CDHA by focal points, extension of citoplasmatic zones represented by both

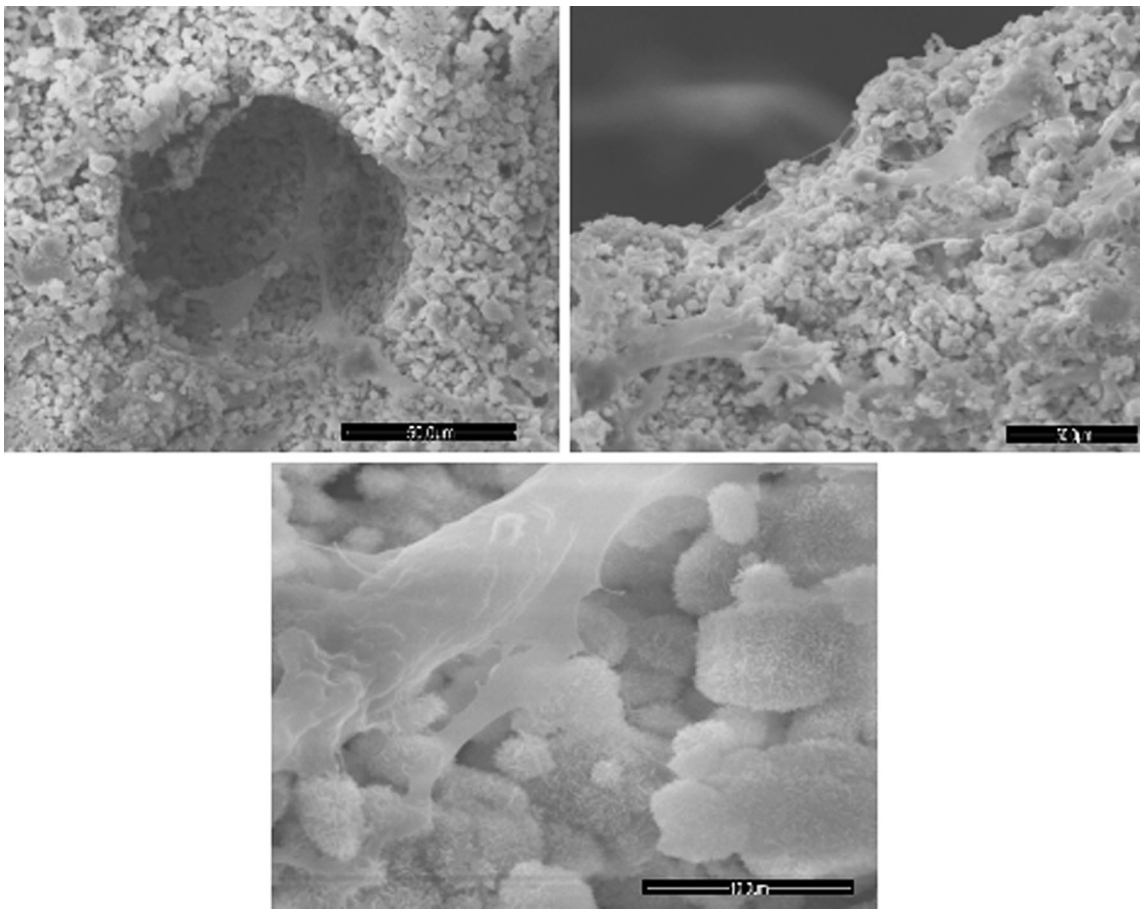

Fig. 8 SEM micrographs showing morphology of hMSC on substrates after 14 days of culture

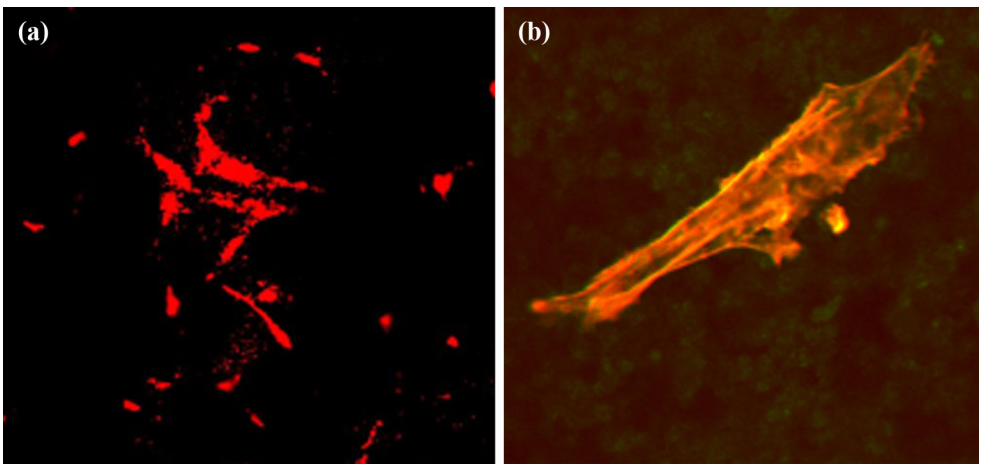

Fig. 9 Cell morphology and cytoskeleton organization of hMSC performed with phalloidine assay after 14 days of culture

cylindrical and thin zones named philopodia, and thick and elongated structures (lamellopodia) responsible of cellular morphology and orientation. Confocal analysis in Fig. 9 confirms SEM observation: after 14 days culture, cells have homogeneously colonized the whole inner macroporosity of the scaffold, and are fine spread on the surface. Cells result sensitive to topological cues concentrating their distribution around pores, confirming porosity as preferential sites for cells adhesion. The particular in Fig. 9b confirms that cells are stretched and adhere by multifocal points to the surface: actin filaments are structured in well-defined stress fibers and oriented in a parallel direction

following the main cellular axis and the multifocal points that allow cells adhering on nano CDHA crystals are defined.

5 Discussion

A forefront approach of bone tissue engineering involves the development of biomaterials directly injectable into the injury sites to gain minimally invasive surgical procedures [3, 5]. The last decade has witnessed a burgeoning development of injectable bone analogues, able to recapitulate a 3D microenvironment by an appropriate recreation of the in vitro chemical, mechanical and biological dynamic interplays. In this contest injectable calcium phosphate cements have been regarded as promising bone-defect repair materials, because of their similarity to the mineral phase of bone, the ability of setting in situ and being recognized and successfully integrated into natural tissue. CPCs possess high tissue compatibility and osteoconductivity, but the restriction of their use is their brittle nature, poor mechanical strength, lack of macroporosity and low porosity degree, responsible of their slow resorption rate [6, 7]. The combination of CPCs with biopolymers has a dual purpose: the improvement of mechanical and morphological properties of the composite, and enhancing the osteoconductive properties of polymers. The current study has been devoted to the fabrication of an injectable bone analogue by the versatile use of foamed gelatin gel. The clear use of gelatin relies on its similarity with collagen and its features such as biocompatibility, the ability of being resorbable in vivo, its processability due to thermosensitive character, its amphiphilic aspect intrinsically connected with foamed ability. Here, by tuning these properties, the biopolymer can be more stable at body temperature, completely foamed, without any residuals that denaturate scaffold or damage cells, and homogeneously mixed to CPC powder, as confirmed by rheological analysis. Among the manifold drawbacks resulting from the cement injection, the primary ones are the hardening and phase separation into the syringe and the lack of cohesion into the injection sites. Qualitatively, adequate cement must possess detailed requirements in terms of rheological features, which must be specific depending on the clinical step. More specifically, during the preparation and over the injection viscous properties are highly desirable, encouraging the flow into the syringe needle and hindering both phase separation and hardening into the syringe. Differently, in situ must dominate the elastic-like behaviour, which allows the cement remaining into the injection site adapting to cavity shape. Interestingly, the cement developed in this study is a composite, where the presence of foamed biopolymer improves the full injection of the cement respect to the cement with unfoamed gelatin, and the injection percentage is much higher than that of HCem, that hardens into the syringe. The good injectability of the cement relies upon a viscous behaviour (G”>G’) that ensures the flow throughout the needle, but 7 min. after the injection, it switches from a viscous to an elastic character (G’>G”), as confirmed by the evolution of the moduli performed by rheological analysis. Moreover, in the cement paste, the interaction among the positive charges of cement Ca^{++} and the carboxylic groups of gelatin and the electrostatic interactions, revealed by FTIR study, renders a stable three dimensional network able to better store elastic energy during the shear deformation without disintegrating. The presence of the polymeric phase, crosslinked by physical entanglements among the chains and the crystal of α-TCP and HA, produces a strong network with reduced motility and the structure cannot flowing out the injection site. Noteworthy, the amount of water contained into the polymeric phase is as much as necessary to allow the hardening of the cement, in this way the paste can be defined as a self-setting system. The hydrolysis process that lead to the formation of CDHA precipitation, as corroborate by ESEM analysis, takes place in the first 24 h and evolved as confirmed by the precipitation of needle-like CDHA crystals depicted by SEM analysis and by the spectra of X-ray, characterised by the typical CDHA peaks. A crucial requirement of a successfully bone ECM analogue is represented by the topography of the surface, that is a regulator of cell adhesion and motility [9]. The cells are sensitive to surface discontinuity of nanometric and micrometric dimension, which permit all the chemical and physical interactions among analogue surface and membrane receptors needed for attachment, migration and material colonization. From our findings, it can be noticed a network with morphological features that resemble the bone histoarchitecture: the composite exhibits an interconnected porosity homogeneously distributed and the presence of acicular nano-crystals of CDHA covering the pore surfaces, that ensure preferential sites for cell adhesion and migration and regulate nutrient supply and waste removal. As corroborate by SEM and CLSM images, the presence of needle-like crystals ensures anchoring sites for cells that are well spread on CDHA crystals and onto the wall pores. Moreover, the ability of the cement to promote the biological activity is also correlated to the synergistic interaction among topography and chemistry. Indeed, the wettability strongly influences cellular activity. The outstanding wettability of the cement surface, related to sample’s hydrophilicity, is due to double aspect: the increased porosity and the presence of carboxylic and amine groups of gelatin, which improve the cellular integrin based recognition of RGD. An essential criteria for the success of the injectable bone analogue is its ability to

withstand loads, providing the temporary mechanical support. The measurements of compressive properties of the cement were found to be within the physiological range. In particular, the value of elastic modulus matches the modulus of natural sponge bone tissue [4]. The engineered scaffold can withstand loads similar to those of natural tissue, provides temporary mechanical support and transfers mechanical stimuli to the progenitor cells adequate to produce new ECM. As expected, according to these promising results, the composite substrates have positive effect on cellular behaviour: MG63 proliferate on the substrates and after 14 days are viable. The protein inclusion enhances the hMSCs recognition, improving the cell colonization of the scaffold and the proliferation. After 14 days cells are well spread into and around pores walls and differentiate toward the osteogenic lineage. Concerning evaluation of the in vitro osteoblastic differentiation, results of RT-PCR and immunostaining show high levels of osteoblastic markers in presence of osteogenic medium and without any osteogenic signal. Cells "feel" the features of materials and reply developing the osteoblastic phenotype confirming that the substrate exhibits osteoinductive and osteoconductive features supporting the osteogenic differentiation of cells. The summary of promising findings demonstrate that foamed gelatin creates a bioactive pathway for guiding cellular recognition and enhancing cell proliferation and differentiation down the osteogenic lineage. The injectable bone analogue possesses specific microarchitecture and mechanical properties able to provide temporary mechanical support and withstand loads able to induce benefits in bone tissue engineering.

6 Conclusion

In this work the engineering of injectable cements, able to simulate the bone's native microenvironment that mimics the topological and microstructural features of bone tissue, has been studied. The selection of gelatin B as foaming agent give rise a final material with interconnected micro and macro porosity where cells perfuse throughout and differentiation of hMSC takes place. Gelatin presence plays the role of cohesion promoter of the paste and increases cement injectability. Moreover, the foamed biopolymer modulates cement mechanical properties, in terms of an excellent degree of plasticity, without interfering with CDHA precipitation, conferring it topological aspects that positively influence the dynamic crosstalks among cells and material. The steadily cellular response represented by good adhesion, proliferation and differentiation proves the positive effect of the use of foamed gelatin in the fabrication of scaffolds with a bioactive pathway. These results demonstrate the potentiality of the cement to recreate a spatially organized structure that resembles the bony ECM functions, suggesting their successful use of in bone regeneration.

Acknowledgments This study was financially supported by the SmartCap Project FP6-STREP NMP3-CT-2005-013912. The authors wish to thank Dr. M. Colella for his precious assistance with SEM and ESEM analysis, Dr. A. Scala for contact angle measurements and Dr. S. Zeppetelli for biological assistance.

References

1. Drumheller P, Hubbell J. The biomedical engineering handbook. Boca Raton: CRC Press LLC; 2000.
2. Kim HW, Song JH, et al. Nanofiber generation of gelatin-hydroxyapatite biomimetics for guided tissue regeneration. Adv Funct Mater. 2005;15:1988–94.
3. Pasquier G, Flautre B, Blary MC, Anselme K, Hardouin P. Injectable percutaneous bone biomaterials: an experimental study in a rabbit model. J Mater Sci Mater Med. 1996;7:683–90.
4. Guarino V, Causa F. Ambrosio L Bioactive scaffolds for bone and ligament tissue. Expert Rev Med Devices. 2007;3:405–18.
5. Lewis G. Injectable bone cements for use in vertebroplasty and kyphoplasty: state of the art review. J Biomed Mater Res B. 2005;76:456–68.
6. Ignjatovic N, Tomic S, Dakic M, Miljkovic M, Plavsic M, Uskokovic D. Synthesis and properties of hydroxyapatite/poly-L-lactide composite biomaterials. Biomaterials. 1999;20:809–16.
7. Cerrai P, Guerra GD, Tricoli M, Krajewski A, Ravaglioli A, Martinetti R, Dolcini L, Fini M, Scarano A, Piattelli A. Periodontal membranes from composites of hydroxyapatite and bioresorbable block copolymers. J Mater Sci Mater Med. 1999;10:677–82.
8. Zoulgami M, Lucas A, Briard P, Gaude J. A self-setting single-component calcium phosphate cement. Biomaterials. 2001;22:1933–7.
9. Hyakuna K, Yamamuro T, Kotoura Y, et al. The influence of calcium phosphate ceramics and glass-ceramics on cultured cells and their surrounding media. J Biomed Mater Res. 1989;9:1049–66.
10. Millot JM, Allam N, Manfait M. Study of the secondary structure of proteins in aqueous solutions by attenuated total reflection Fourier transform infrared spectrometry. Anal Chim Acta. 1994;295:233–41.
11. Bigi B, Bracci B, Panzavolta S. Effect of added gelatin on the properties of calcium phosphate cement. Biomaterials. 2004;25:2893–9.
12. Changa MC, DeLonga R. Calcium phosphate formation in gelatin matrix using free ion precursors of Ca^{2+} and phosphate ions. Dent Mater. 2009;25:261–8.
13. Barbetta A, Dentini M, De Vecchis MS, Filippini P, Formisano G, Caiazza S. Scaffolds based on biopolymeric foams. Adv Funct Mater. 2005;75:118–24.
14. Espanol M, Portillo J, Manero JM, Ginebra MP. Investigation of the hydroxyapatite obtained as hydrolysis product of α-tricalcium phosphate by transmission electron microscopy. CrystEngComm. 2010;12:3318–26.
15. Xin X, Borzacchiello A, Netti PA, Ambrosio L, Nicolais L. Hyaluronic-acid-based semi-interpenetrating materials. J Biomater Sci. 2004;9:1223–36.
16. Van Den Bulcke AI, Bogdanov B, De Rooze N, Schacht EH, Cornelissen M, Berghmans H. Structural and Rheological

Properties of Methacrylamide Modified Gelatin Hydrogels. Biomacromolecules. 2000;1:31–8.
17. Leone G, Barbucci R, Borzacchiello A, Ambrosio L, Netti PA, Migliaresi C. Preparation and physico-chemical characterization of microporous polysaccaridic hydrogels. J Mater Sci Mater Med. 2004;15:463–7.
18. Xu LC, Siedlecki CA. Effects of surface wettability and contact time on protein adhesion to biomaterial surfaces. Biomaterials. 2007;28:3273–83.
19. Tzoneva R, Faucheux N, Groth T. Wettability of substrata controls cell–substrate and cell–cell adhesions. Biochim Biophys Acta. 2007;1770:1538–47.
20. Watanabe T. Wettability of ceramic surfaces-A wide range control of surface wettability from super hydrophilicity to super hydrophobicity, from static wettability to dynamic wettability. J Cer Soc Jpn. 2009;117:1285–92.
21. Bigi A, Boanini E, Rubini K. Hydroxyapatite gels and nanocrystals prepared through a sol–gel process. J Solid State Chem. 2004;177:3092–8.
22. Nociari M, Shalev A, Benias P, Russo C. A novel one-step, highly sensitive fluorometric assay to evaluate cell-mediated cytotoxicity. J Immunol Method. 1998;213:157–67.
23. Goegan P, Johnson G, Vincent R. Effects of serum protein and colloid on the Alamar blue assay in cell cultures. Toxic Vim. 1995;9:257–66.
24. Betz MW, Modi PC, Caccamese JF, Coletti DP, Sauk JJ, Fisher JP. Cyclic acetal hydrogel system for bone marrow stromal cell encapsulation and osteodifferentiation. J Biomed Mater Res. 2008;86A:662–70.
25. Moreau JL, Xu HHK. Mesenchymal stem cell proliferation and differentiation on an injectable calcium phosphate-chitosan composite scaffold. Biomaterials. 2009;30:2675–82.
26. Martin R. Toward a unifying theory of bone remodeling. Bone. 2000;26:1–6.
27. Nicholson PHF, Cheng X. G Lowet. Structural and material mechanical properties of human vertebral cancellous bone. Med Eng Phys. 1997;19:729–37.
28. Lopes M, Monteiro F, Santos J, Serro A, Saramago B. Hydrophobicity, surface tension, and zeta potential measurements of glass-reinforced hydroxyapatite composites. J Biomed Mater Res. 1999;45:370–5.
29. Navarro M, Engel E, Planell JA, Amaral I, Barbosa M, Ginebra MP. Surface characterization and cell response of a PLA/CaP glass biodegradable composite material. J Biomed Mater Res A. 2007;85:477–86.
30. Li Z, Yubao L, Xuejiang W, Jie W, Xuelin P. Studies on the porous scaffold made of the nano-HA composite. J Mater Sci. 2005;40:107–10.
31. Chang MC, Kim UK, Douglas WH. Modification of Hydroxyapatite/Gelatin Nanocomposite Using Polyacrylamide. J Biomater Sci Polym Ed. 2009;20:363–75.
32. Mirkin NG, Krimm S. Amide III Mode φ, ψ Dependence in Peptides: a Vibrational Frequency Map. J Phys Chem A. 2002;106:3391–4.
33. Chang MC, Koa CC, Douglas WH. Conformational change of hydroxyapatite/gelatin nanocomposite by glutaraldehyde. Biomaterials. 2003;24:3087–94.
34. Hashim DM, Che Man YB, Norakasha R, Shuhaimi M, Salmah Y, Syahariza ZA. Potential use of Fourier transform infrared spectroscopy for differentiation of bovine and porcine gelatins. Food Chem. 2010;118:856–60.
35. Fischer G, Cao X, Cox N, Francis M. The FTIR spectra of glycine and glycylglycine zwitterions isolated in alkali halide matrices. J Chem Phys. 2005;313:39–49.
36. Siddharthan A, Seshadri SK, Sampath Kumar TS. Rapid synthesis of calcium deficient hydroxyapatite nanoparticles by microwave irradiation. Trends Biomater Artif Organs. 2005;18:110–4.
37. Siddharthan A, Sampath Kumar TS, Seshadri SK. Synthesis and characterization of nanocrystalline apatites from eggshells at different Ca/P ratios. Biomed Mater. 2009;39:439–68.
38. Almirall A, Larrecq G, Delgado JA, Martınez S, Planell JA, Ginebra MP. Fabrication of low temperature macroporous hydroxyapatite scaffolds by foaming and hydrolysis of an α-TCP paste. Biomaterials. 2004;25:3671–80.
39. Liu Y, Hou D, Wang G. A simple wet chemical synthesis and characterization of hydroxyapatite nanorods. Mat Chem Phys. 2004;86:69–73.
40. Causa F, Netti PA, Ambrosio L. A multi-functional scaffold for tissue regeneration: the need to engineer a tissue analogue. Biomaterials. 2007;28:5093–9.